Nano World Journal

https://doi.org/10.17756/nwj.2025-144

Research Article

Open Access

Tuning Electronic and Optical Properties in $Co_8Cr_{16}O_{24}$ through Bismuth and Zirconium Doping

Rafat M. Ibrahim*

Department of Physics, Faculty of Science, Taibah University, Saudi Arabia

***Correspondence to:**
Rafat M. Ibrahim
Department of Physics,
Faculty of Science,
Taibah University,
Saudi Arabia.
E-mail: rtum@taibahu.edu.sa

Received: September 01, 2025
Accepted: September 09, 2025
Published: September 12, 2025

Citation: Ibrahim RM. 2025. Tuning Electronic and Optical Properties in $Co_8Cr_{16}O_{24}$ through Bismuth and Zirconium Doping. *NanoWorld J* 11(2): 26-31.

Copyright: © 2025 Ibrahim. This is an Open Access article distributed under the terms of the Creative Commons Attribution 4.0 International License (CC-BY) (http://creativecommons.org/licenses/by/4.0/) which permits commercial use, including reproduction, adaptation, and distribution of the article provided the original author and source are credited.

Published by United Scientific Group

Abstract

Using density functional theory (DFT) via the all-electron, full-potential linearized augmented plane wave (LAPW) approach implemented in the ELK code, we investigate the electronic structure and optical properties of bulk $Co_8Cr_{16}O_{24}$ along with its doped derivatives $Co_8Cr_{15}BiO_{24}$ and $Co_8Cr_{15}ZrO_{24}$. The bulk material exhibits intrinsic semiconductor behavior with an effective band gap of roughly 0.7 eV, arising from distinct spin-polarized contributions—where the spin-up states dominate the valence band and the spin-down states define the conduction band. In the bismuth (Bi)-substituted compound, the band gap narrows and becomes indirect, as the conduction band edge shifts to the L point and the valence band edge to the Γ point, while the Fermi level remains centrally positioned. In contrast, zirconium (Zr) substitution not only further reduces the band gap but also shifts the Fermi level towards the conduction band, inducing n-type behavior by acting as an electron donor. Optical analyses indicate that although all samples show comparable refractive index behavior at wavelengths below 800 nm, significant differences emerge at longer wavelengths. Specifically, Bi doping enhances both the refractive index and reflectance, while Zr doping initially lowers the refractive index before it rises markedly in the infrared range. These findings illustrate that selective doping effectively tailors the electronic and optical properties of $Co_8Cr_{16}O_{24}$ based materials, presenting promising routes for advanced semiconductor and optoelectronic applications.

Keywords

Density functional theory, Optical properties, Doping

Introduction

The tailored modification of semiconductor materials through doping strategies has become a central theme in modern materials science [1-5]. Doping is instrumental in manipulating the band structure and electrical properties of semiconductors, thereby enhancing their performance for applications in photovoltaics, sensors, and optoelectronic devices. Transition metal oxides are particularly attractive in this regard due to their diverse electronic interactions and strong correlations. In this study, we focus on $Co_8Cr_{16}O_{24}$, an intrinsic semiconductor exhibiting a balanced spin-polarized electronic structure with an effective band gap of approximately 2 eV [6]. Investigating this material under selective doping with Bi and Zr offers promising avenues for tuning both its electronic and optical properties [7, 8].

A wealth of research in physical science has indicated the profound impact that doping can have on physical and chemical properties of materials [9, 10]. In III-V semiconductors such as gallium arsenide (GaAs), the incorporation of Bi has been shown to reduce the band gap through the hybridization of Bi orbitals

with the host electronic states, while maintaining a balanced intrinsic character [11]. Similar effects have been reported in $BiFeO_3$ thin films, where Bi incorporation not only narrowed the band gap but also modified the optical responses without severely altering the charge carrier balance [12]. Complementarily, Zr doping has received considerable attention for its ability to introduce donor states in semiconductor oxides. Studies have demonstrated that substituting a host atom with Zr not only reduces the band gap but also shifts the Fermi level toward the conduction band, contributing to an n-type semiconducting behavior [13, 14].

$Co_8Cr_{16}O_{24}$ serves as an excellent candidate to explore these doping effects due to its intrinsic semiconductor properties [15]. In its bulk form, the material is characterized by a centrally positioned Fermi level within an approximately 0.7 eV gap, with the spin-up contribution predominating at the valence band edge and spin-down states defining the conduction band edge. This balanced electronic configuration provides a robust foundation for examining how extrinsic dopants can alter the material's properties. In particular, the substitution of chromium (Cr) with Bi and Zr has emerged as an effective strategy for inducing significant modifications in the electronic band structure and optical responses.

Recent computational studies utilizing DFT have proven invaluable for elucidating these modifications. In our work, the all-electron, full-potential LAPW method [16], as implemented in the ELK code [17], is employed to achieve a high degree of accuracy. This approach treats both core and valence electrons without resorting to pseudopotentials, thereby capturing the subtle interactions that govern the electronic structure in complex oxides. Such precision is essential for accurately modeling the spin-polarized characteristics of $Co_8Cr_{16}O_{24}$ and predicting the impact of dopant-induced perturbations.

Experimental and computational literature on doping in semiconductors consistently highlights the contrasting effects induced by different dopants. For example, when a Cr atom in $Co_8Cr_{16}O_{24}$ is replaced by Bi to form $Co_8Cr_{15}BiO_{24}$, studies have observed a marked narrowing of the band gap. This change is accompanied by a transition from a nearly direct to an indirect band gap configuration, with the conduction band of minimum shifting from one high-symmetry point to another. Importantly, the position of the Fermi level remains nearly centered, indicating that the overall balance of charge carriers is preserved despite significant modifications to the band structure. This observation is in accordance with findings from Bi-doped semiconductor systems, where orbital interactions serve to perturb the band edges without dramatically altering carrier concentrations [11].

In contrast, the effect of Zr doping in $Co_8Cr_{16}O_{24}$ yields a different electronic response. When a Cr atom is substituted with Zr to form $Co_8Cr_{15}ZrO_{24}$, the dopant acts as a donor, shifting the Fermi level toward the conduction band and thereby giving rise to n-type semiconducting behavior. This donor effect is accompanied by a further reduction in the band gap, which influences not only the electrical conductivity but also the optical properties. In particular, the enhanced free electron concentration in the Zr-doped material significantly modifies its refractive index and reflectance. At shorter wavelengths, similar optical behavior is observed across undoped, Bi-doped, and Zr-doped samples due to strong near-edge electronic transitions. However, at longer wavelengths, these differences become more pronounced. For instance, while the Bi-doped sample exhibits a higher refractive index and increased reflectance—likely due to a narrower band gap and stronger light-matter interactions, the Zr-doped material initially displays a reduced refractive index that later increases sharply in the infrared region. Such behavior underscores the complex interplay between electronic structure and optical response in doped semiconductor oxides [13, 14].

The optical properties of semiconductors are critical for their application in devices such as LEDs, photo detectors, and solar cells. The refractive index, in particular, is closely tied to a material's electronic structure, with modifications in the band gap often resulting in an altered polarizability. Enhanced polarizability generally leads to a higher refractive index, which has been experimentally observed in several Bi-doped systems [18]. Conversely, the presence of additional free electrons in Zr-doped systems can lead to a complex spectral dependence of the refractive index, reflecting both the reduction in band gap and the increased electron density available for optical transitions. These insights offer a direct link between computational predictions and the practical enhancements observed in optoelectronic properties.

In light of these previous studies, the present investigation seeks to provide a comprehensive understanding of how Bi and Zr doping distinctly alter the electronic and optical properties of $Co_8Cr_{16}O_{24}$. By leveraging advanced DFT methods and a full-potential LAPW framework, we systematically characterize the inherent semiconducting behavior of the bulk material and quantify the modifications ensuing from targeted dopant substitutions. Our work aims to bridge the gap between theoretical predictions and experimental observations in transition metal oxide semiconductors, offering valuable guidance for the future design of materials with tailored functionalities.

Understanding the microscopic mechanisms and macroscopic consequences of doping in $Co_8Cr_{16}O_{24}$ not only deepens the fundamental scientific insight into semiconductor physics but also paves the way for the development of next-generation electronic and photonic devices. The comparative study of Bi and Zr dopants presented here reinforces the idea that while both dopants reduce the band gap, their mechanisms of action diverge: Bi primarily alters the band structure through orbital interactions, whereas Zr effectively acts as an electron donor, modifying carrier concentrations and shifting the Fermi level. Such nuanced differences underline the importance of selecting appropriate dopants to achieve specific material properties.

In summary, the integration of electronic structure and optical property analyses in the lightly doped $Co_8Cr_{16}O_{24}$ system represents a crucial step toward harnessing the full potential of transition metal oxides for advanced semiconductor applications. The results of this study are expected to contribute significantly to the field by providing a clearer understanding of the doping mechanisms at play, thereby guiding researchers in the design of materials optimized for superior electronic and optical performance.

Calculation methods

The structural optimization of the studied material was performed using DFT as implemented in the Quantum ESPRESSO (QE) package [19]. Full structural relaxation was carried out, allowing both the lattice parameters and atomic positions to converge to their equilibrium values. The Perdew-Burke-Ernzerhof (PBE) exchange-correlation functional [20] within the generalized gradient approximation (GGA) was employed for these calculations. Ultrasoft pseudopotentials were used to represent the electron-ion interactions. To account for the strong on-site Coulomb interactions of the d electrons in the transition metal elements (Co and Cr), a Hubbard U correction was applied within the GGA + U formalism [21]. The Hubbard U correction in DFT calculations accounts for strong on-site Coulomb interactions, particularly in transition metal elements, by introducing an additional parameter (U) that modifies the potential felt by electrons on the same atomic site. This correction improves the description of localized states, such as those in d-orbitals, which are poorly treated by standard DFT functionals. It enhances the accuracy of simulating electronic properties, including band gaps and magnetic behavior, by better capturing the effects of electron localization and correlation. The values of the effective Hubbard parameters (U) and the Hund's exchange parameters (J) were adopted to be consistent with those used in the subsequent ELK calculations: for Co (l = 2), U = 0.13597 Ry and J = 0.00 Ry and for Cr (l = 2), U = 0.12201 Ry and J = 0.00 Ry. The convergence criteria for structural relaxation were set to the default force threshold within QE. The use of the PBE functional within the GGA + U framework enhances the accuracy of DFT calculations by addressing the limitations of standard DFT in describing localized states. The GGA + U approach combines the GGA with the Hubbard U correction, which accounts for strong on-site Coulomb interactions, particularly in transition metal elements. This correction modifies the potential felt by electrons on the same atomic site, improving the description of localized states, such as d-orbitals. As a result, the PBE functional within this framework provides more accurate simulations of electronic properties, including band gaps and magnetic behavior, by better capturing electron localization and correlation.

Following the structural optimization, a more detailed investigation of the electronic, optical, and magnetic properties was conducted using the full potential LAPW method as implemented in the ELK code [17]. The optimized crystal structure obtained from the QE calculations was used as the input for the ELK calculations. The exchange-correlation effects were again treated using the PBE functional within the GGA + U framework, with the same U and J parameters for Co and Cr as specified above, and employing the around mean field double counting correction (dft + u = 2). Spin-polarized calculations were performed (spinpol = .true.) to account for potential magnetic ordering, with a small magnetic field of -0.01 Ry applied along the z-axis (bfieldc) to break initial symmetry and facilitate convergence to a magnetic ground state. Broyden's mixing scheme (mixtype = 3) was used to accelerate the self-consistent field convergence. A relatively dense 4 × 4 × 4 k-point mesh (ngridk) was employed for Brillouin zone sampling to ensure accurate integration. A sufficient number of empty states (nempty = 24) were included to accurately calculate the electronic band structure, density of states (DOS), optical properties and magnetic moments. The wave functions were expanded using a plane-wave cutoff determined by Rmt × kmax, where Rmt is the smallest muffin-tin radius and kmax is the maximum wave vector. The value of maxthd1 = −4 likely relates to the precision and convergence thresholds within the ELK code. The lattice vectors (avec) and the scaling factor (scale) define the dimensions and shape of the supercell used in the calculations, with the atomic positions provided in fractional coordinates within this supercell.

This two-step approach, utilizing QE for efficient structural optimization and ELK for high-accuracy property calculations with consistent GGA + U parameters, provides a robust framework for investigating the material's fundamental characteristics.

Results and discussion

Figure 1 shows the electronic band structure and DOS for the bulk $Co_8Cr_{16}O_{24}$ supercell, calculated using the ELK LAPW, as explained in the calculation method. The findings indicate that $Co_8Cr_{16}O_{24}$ functions as an intrinsic semiconductor, showing a distinct band gap. The Fermi level, set as the zero-energy reference, is located about halfway within this band gap, suggesting a balanced electronic structure. The observed effective band gap is approximately 0.7 eV, resulting from the overlap of different-sized band gaps identified in the spin-up (around 3 eV) and spin-down (around 2 eV) DOS plots, which appear on either side of the band structure. These DOS plots indicate that the valence band edge main-

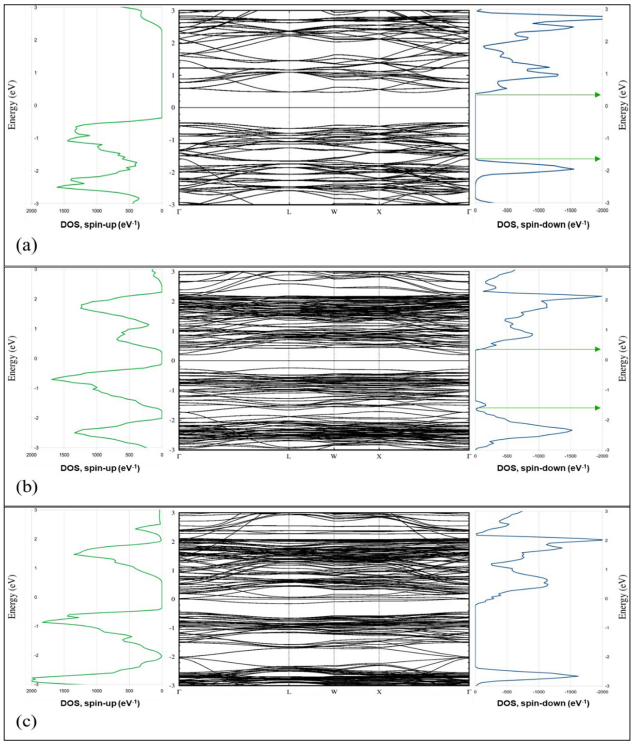

Figure 1: The band structure and DOS for **(a)** bulk $Co_8Cr_{16}O_{24}$, **(b)** Bi doped $Co_8Cr_{15}BiO_{24}$, and **(c)** Zr doped $Co_8Cr_{15}ZrO_{24}$.

ly comes from the spin-up states, while the conduction band edge mainly comes from the spin-down states.

Figure 2 illustrates how substituting one Cr atom with Bi affects the electronic structure, resulting in the compound $Co_8Cr_{15}BiO_{24}$. This substitution significantly lowers the band gap, while the Fermi level remains almost centered within the gap. Therefore, adding Bi primarily changes the size of the band gap, maintaining the intrinsic semiconductor properties without significantly altering the type or number of charge carriers. Similar findings have been reported, where incorporating Bi atoms into other semiconductor materials like GaAs led to a smaller band gap due to interactions between Bi orbitals and the host material orbitals, without greatly affecting the type or quantity of charge carriers [11]. When comparing figure 2 to figure 1, the DOS plots for $Co_8Cr_{15}BiO_{24}$ show that the band gap and the positions of the valence and conduction band edges for the spin-down states are similar to those seen in bulk $Co_8Cr_{16}O_{24}$. One clear difference is that, unlike the bulk material, which has a nearly direct band gap around the W point, the Bi-substituted material exhibits an indirect band gap. In this case, the conduction band edge is situated at the L point, while the valence band edge is at the gamma point.

In contrast, figure 3 presents the electronic structure when Cr is replaced by Zr, producing $Co_8Cr_{15}ZrO_{24}$. The substitution of Zr not only reduces the band gap but also moves the Fermi level closer to the conduction band, converting the semiconductor into an n-type material. This indicates that Zr atoms act as electron donors, increasing the electron concentration in the conduction band. Similar n-type doping behavior from Zr substitution has been observed in earlier studies involving metal oxides and alloy materials, where Zr doping typically improved electrical conductivity by boosting electron concentration and overall electrical performance [13, 14]. Unlike the Bi-substituted material, the band edges in the Zr-substituted structure are located at the L point for the valence band and at the gamma point for the conduction band.

Figure 2 shows how the refractive index changes with wavelength for bulk $Co_8Cr_{16}O_{24}$ ("bulk") compared to Bi-doped ($Co_8Cr_{15}BiO_{24}$) and Zr-doped ($Co_8Cr_{15}ZrO_{24}$) materials. At shorter wavelengths (below about 800 nm), all three materials exhibit similar behavior, with a noticeable increase in refractive index due to strong interactions with incoming light near the band gap. At intermediate and longer wavelengths (approximately 800 nm to 8000 nm), differences appear among the samples. The bulk material stabilizes with a refractive index around 2.5. The Bi-doped sample shows a significant increase, stabilizing near 3.5, reflecting stronger light interactions due to changes in electronic structure caused by Bi doping. This is linked to a narrower band gap, allowing for greater polarizability. In contrast, Zr doping initially lowers the refractive index below that of both the bulk and Bi-doped samples (around 800 – 2000 nm). However, at longer wavelengths (beyond about 2000 nm), the refractive index for the Zr-doped sample increases significantly, exceeding both other samples. This may result from additional free electrons from Zr doping, enhancing interactions with infrared radiation.

The plot shows the reflectance variation with wavelength

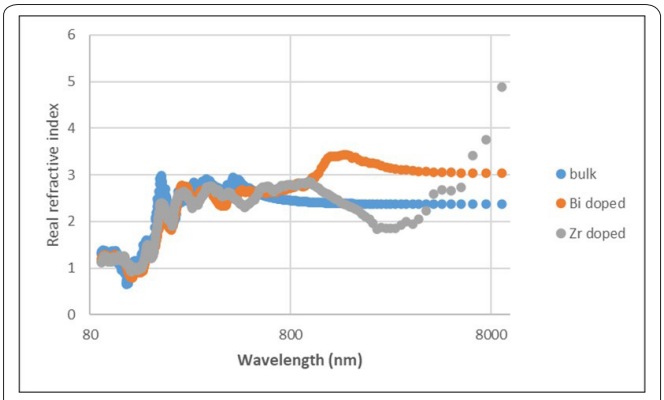

Figure 2: The calculated refractive index vs wavelength for the bulk and doped structures.

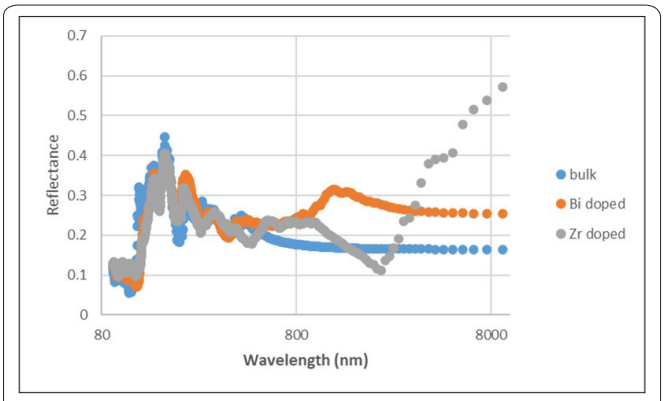

Figure 3: The calculated reflectance vs wavelength for the bulk and doped structures.

for bulk $Co_8Cr_{16}O_{24}$ ("bulk") and its Bi-doped ($Co_8Cr_{15}BiO_{24}$) and Zr-doped ($Co_8Cr_{15}ZrO_{24}$) versions. At wavelengths below 800 nm, all three materials display similar reflectance patterns with multiple peaks, caused by strong electronic transitions near the band edges, increasing reflectance due to the interaction between photons and electrons. Beyond 800 nm, differences become apparent. The bulk material maintains a stable reflectance around 0.2. Bi doping raises reflectance to about 0.3 at these longer wavelengths, consistent with a narrowed band gap and a higher refractive index, which enhances light reflectivity. In contrast, the Zr-doped material shows initially lower reflectance in the 800 – 2000 nm range, but it increases significantly beyond 2000 nm, exceeding both bulk and Bi-doped materials. This increase is likely due to free electrons from Zr doping, enhancing interactions with long-wavelength (infrared) photons. This aligns with findings that Zr doping improves conductivity and alters optical reflectance, particularly in the infrared range.

It is worth pointing out the key differences in the electronic structures of $Co_8Cr_{16}O_{24}$, $Co_8Cr_{15}BiO_{24}$, and $Co_8Cr_{15}ZrO_{24}$ are primarily related to the substitution of different elements (Bi and Zr) for Cr in the $Co_8Cr_{16}O_{24}$ structure. These substitutions can significantly affect the electronic and magnetic properties of the materials. Specifically:

1. $Co_8Cr_{16}O_{24}$: This compound likely has a high concentration of Cr, which contributes to strong magnetic interactions due to the localized d-orbitals of Cr. The electronic

structure would be characterized by a narrow band gap, influenced by the strong on-site Coulomb interactions between Cr d-electrons.

2. $Co_8Cr_{15}BiO_{24}$: The substitution of Bi for one Cr atom introduces a different electronic environment. Bi has a different electronic configuration ($6s^26p^3$) compared to Cr ($3d^54s^1$), which can lead to changes in the band structure. The presence of Bi can result in a modified band gap and potentially alter the magnetic properties due to the different orbital interactions and spin contributions.

3. $Co_8Cr_{15}ZrO_{24}$: The substitution of Zr for one Cr atom introduces a different electronic configuration ($4d^25s^2$ for Zr compared to $3d^54s^1$ for Cr). Zr's larger atomic size and different orbital interactions can lead to a shift in the electronic structure, potentially affecting the band gap and magnetic properties. The substitution of Zr may also reduce the overall magnetic moment compared to Cr, as Zr has a lower number of unpaired electrons.

Conclusion

This study demonstrates that selective doping of $Co_8Cr_{16}O_{24}$ with Bi and Zr effectively modifies the electronic and optical properties of this intrinsic semiconductor. The undoped material exhibits a balanced spin-polarized electronic structure with an effective band gap of approximately 0.7 eV and a centrally positioned Fermi level.

Bi substitution in $Co_8Cr_{15}BiO_{24}$ primarily narrows the band gap while maintaining intrinsic semiconductor characteristics. The doping transforms the nearly direct band gap of the bulk material into an indirect configuration, with the conduction band minimum shifting to the L point and the valence band maximum to the Γ point. Importantly, the Fermi level position remains largely unchanged, preserving the balance between charge carriers.

In contrast, Zr doping in $Co_8Cr_{15}ZrO_{24}$ not only reduces the band gap but also shifts the Fermi level toward the conduction band, inducing n-type semiconducting behavior. This electron donor effect significantly alters the material's electronic properties by increasing the electron concentration in the conduction band.

The optical properties reflect these electronic structure modifications. While all materials exhibit similar refractive index behavior at wavelengths below 800 nm, substantial differences emerge at longer wavelengths. Bi doping enhances both the refractive index and reflectance due to increased polarizability from the narrowed band gap. Zr doping initially decreases the refractive index but leads to significant enhancement in the infrared region, attributed to enhanced free electron interactions with long wavelength photons.

These findings establish that targeted doping strategies can systematically tune the electronic and optical properties of $Co_8Cr_{16}O_{24}$-based materials. The distinct mechanisms of action—orbital hybridization for Bi vs electron donation for Zr—provide precise control over material characteristics. This work contributes to the fundamental understanding of doping effects in transition metal oxides and offers promising pathways for developing advanced semiconductor and optoelectronic applications.

Acknowledgements

I would like to express my sincere gratitude to Prof. M. B. Mohamed and Dr. M. A. H. Khalafalla at Taibah University for their valuable discussions, constructive feedback, and continuous support throughout this research. Their guidance has been instrumental in shaping and refining this work. I also wish to acknowledge Taibah University for providing the academic environment and resources that made this study possible.

Conflict of Interest

The author declares that there are no conflicts of interest regarding the publication of this paper.

References

1. Kushare SS, Bobade VD, Tope DR, Borhade AV. 2021. $CoCr_2O_4$@GeO_2@ZnO core-shell nanoparticle as a novel recoverable catalyst: preparation, characterization and photocatalytic degradation of basic fuchsin dye. *J Indian Chem Soc* 98(12): 100239. https://doi.org/10.1016/j.jics.2021.100239
2. Shafique R, Rani M, Janjua NK, Arshad M, Batool K, et al. 2024. Electrifying energy storage by investigating the electrochemical behavior of $CoCr_2O_4$/graphene-oxide nanocomposite as supercapacitor high performance electrode material. *Heliyon* 10(23): 1-11. https://doi.org/10.1016/j.heliyon.2024.e40702
3. Jabeen S, Ahmad A, Kumar A, Alsalhi SA, Makasana J, et al. 2025. Preparation of nano-composite of $CoCr_2O_4$ with rGO by solvothermal method for water splitting. *Diam Relat Mater* 154: 112167. https://doi.org/10.1016/j.diamond.2025.112167
4. Choudapur VH, Jagadeesha AV, Tudorache F, Ayachit N, Shaikh SF, et al. 2024. Structural, optical and humidity sensing performance of lanthanum doped $CoCr_2O_4$ nano-ceramics for sensor applications. *Ceram Int* 50(21): 44056-44067. https://doi.org/10.1016/j.ceramint.2024.08.255
5. Bhagwan J, Han JI. 2024. Synthesis of MWCNT/$CoCr_2O_4$ for high performance aqueous hybrid supercapacitor. *J Energy Storage* 104: 114510. https://doi.org/10.1016/j.est.2024.114510
6. Hitkari G, Sandhya S, Gajanan P, Shrivash MK, Deepak K. 2018. Synthesis of chromium doped cobalt oxide (Cr:Co_3O_4) nanoparticles by co-precipitation method and enhanced photocatalytic properties in the visible region. *J Mater Sci Eng* 7(1): 1-6. https://doi.org/10.4172/2169-0022.1000419
7. Jagadeesha AV, Pasha A, Ubaidullah M, Gupta M, Pandit B, et al. 2023. Rare earth (Sm3+) doped $CoCr_2O_4$ ceramics sensor towards room temperature detection of greenhouse methane gas. *Ceram Int* 49(10): 16174–16181. https://doi.org/10.1016/j.ceramint.2023.01.215
8. Garima, Dhaka S, Singh V, Thakur A, Choudhary BL, et al. 2024. Unraveling the structural and magnetic characteristics of Mg doped $CoCr_2O_4$. *Mater Lett* 377(15): 137550. https://doi.org/10.1016/j.matlet.2024.137550
9. Pruthviraj IS, Radha Krushna BR, Sharma SC, Manjunatha K, Wu SY, et al. 2025. Exploring Mg^{2+} doped $CoCr_2O_4$ nanoparticles: eco-friendly pigments, radiation dosimeters and latent fingerprint visualization. *Mater Sci Eng B* 317: 118217. https://doi.org/10.1016/j.mseb.2025.118217
10. Ghosh MP, Sonkar R, Phukan G, Borah JP, Chowdhury D. 2025. Gd^{3+} doped $CoCr_2O_4$ nanoparticles: tuning of physical properties and optimizing the hyperthermia efficacy. *Nanoscale Adv* 7(6): 1698-1713. https://doi.org/10.1039/d4na00685b

11. Bannow LC, Rubel O, Badescu SC, Rosenow P, Hader J, et al. 2016. Configuration dependence of band-gap narrowing and localization in dilute $GaAs_{1-x}Bi_x$ alloys. *Phys Rev B* 93: 205202. https://doi.org/10.1103/PhysRevB.93.205202

12. Mukherjee S, Gupta R, Garg A, Bansal V, Bhargava S. 2010. Influence of Zr doping on the structure and ferroelectric properties of $BiFeO_3$ thin films. *J Appl Phys* 107: 123535. https://doi.org/10.1063/1.3436593

13. Hou Q, Zhao C, Xu Z. 2016. Effect of Zr doping on the electrical and optical properties of ZnO. *Chem Phys Lett* 658(1): 336-342. https://doi.org/10.1016/j.cplett.2016.06.075

14. Penki TR, Gilady S, Nayak PK, Sclar H, Elias Y, et al. 2021. The effect of synthesis and zirconium doping on the performance of nickel-rich NCM622 cathode materials for Li-ion batteries. *J Solid State Electrochem* 25: 1513-1530. https://doi.org/10.1007/s10008-021-04933-x

15. Wang M, Wang K, Jin Z. 2025. Mixed metal oxides induce directional electron migration to boost $CoCr_2O_4$ photocatalytic hydrogen precipitation activity. *Surf Interfaces* 56(1): 105622. https://doi.org/10.1016/j.surfin.2024.105622

16. Singh DJ, Nordstrom L. 2006. Planewaves, Pseudopotentials, and the LAPW Method. In Springer Science & Business Media. New York, pp 1-134.

17. An All-Electron Full-Potential Linearised Augmented-Planewave (FP-LAPW) Code. [https://sourceforge.net/projects/elk/] [Accessed September 11, 2025]

18. Kizmi J, Ooi PC, Goh BT, Lee MK, Mohd Razip Wee MF, et al. 2020. Bi-doping improves the magnetic properties of zinc oxide nanowires. *RSC Adv* 10(39): 23297-23311. https://doi.org/10.1039/D0RA03816D

19. Giannozzi P, Andreussi O, Brumme T, Bunau O, Nardelli MB, et al. 2017. Advanced capabilities for materials modelling with QUANTUM ESPRESSO. *J Phys Condens Matter* 29(46): 465901. https://doi.org/10.1088/1361-648X/aa8f79

20. Perdew JP, Burke K, Wang Y. 1996. Generalized gradient approximation for the exchange-correlation hole of a many-electron system. *Phys Rev B* 54: 16533. https://doi.org/10.1103/PhysRevB.54.16533

21. Anisimov VI, Aryasetiawan F, Lichtenstein AI. 1997. First-principles calculations of the electronic structure and spectra of strongly correlated systems: the LDA+ *U* method. *J Phys Condens Matter* 9(4): 767. https://doi.org/10.1088/0953-8984/9/4/002